# Resilience-Oriented Two-Stage Restoration Considering Coordinated Maintenance and Reconfiguration in Integrated Power Distribution and Heating Systems

Ke Wang, *Student Member, IEEE*, Yixun Xue, *Member, IEEE*, Mohammad Shahidehpour, *Life Fellow, IEEE*, Xinyue Chang, *Member, IEEE*, Zening Li, *Member, IEEE*, Yue Zhou, *Member, IEEE*, and Hongbin Sun, *Fellow, IEEE*

***Abstract*—The inherent linkage between a power distribution system (PDS) and a district heating system (DHS) necessitates coordinated load restoration after natural disasters. To guarantee optimal load restoration during a recovery process, a coordinated dispatch strategy of the maintenance crew for the PDS/DHS considering the optimal reconfiguration of their respective networks is proposed in this paper. The proposed solution focuses on the intricate mutual interaction of the DHS and PDS and coordinates the fault isolation and service restoration stages. The proposed optimization is modeled as a mixed-integer second-order cone problem (MISOCP), which contains numerous integer variables. To lessen the computational burden, a two-stage acceleration algorithm is proposed, which divides the solution procedure into two stages based on two types of integer variables: load status variables and variables associated with the maintenance path and network topology. Then, the acceleration principles are proposed to determine the load status variables. The effectiveness and accuracy of the proposed model are validated by extensive cases, which demonstrate the performance of the coordinated maintenance and reconfiguration in integrated energy systems for fault recovery.**

***Index Terms*—Integrated power distribution and heating system, coordinated load restoration, maintenance crew, network reconfiguration, two-stage acceleration algorithm.**

## NOMENCLATURE

### A. Indices and Sets

| | |
|---|---|
| $t$ / $c$ | Index of time/ maintenance crew |
| $T_I$ / $T_R$ | Index of fault segmentation stage/ service restoration stage |
| $k^{FP}$ / $k^{FL}$ | Set of damaged pipes in DHS/lines in PDS |
| $k^{pipe}$ / $k^{line}$ | Set of pipes in DHS/lines in PDS |
| $k^{node}$ / $k^{bus}$ | Set of nodes in DHS/buses in PDS |
| $k_{j,n}^{CHP}$ / $k_{j,b}^{CHP}$ | Set of buses/nodes connected to CHP unit $j$ |
| $\Omega^E$ / $\Omega^H$ | Set of root nodes in DHS/root buses in PDS |

### B. Parameters

| | |
|---|---|
| $\Delta T_I$ / $\Delta T_R$ | fault isolation duration/ restoration duration |
| $\underline{\nu}_j$ / $\overline{\nu}_j$ | Upper/lower limits of coefficient between electric and heat output of CHP unit $j$ |
| $f_{ij}$ / $s_{ij}$ | Boolean variable that indicates whether the pipe/line $(i,j)$ is damaged and whether it is equipped with valve/switch |
| $\sigma_j$ / $\gamma_j$ | Coefficient between electricity and heat production of EB $j$ and coefficient between fuel consumption and heat output of HB $j$ |
| $h_j^L$ / $p_j^L$ | Heat/Electric load demand of node/bus $j$ |
| $\underline{h}_j^{CHP}$ / $\overline{h}_j^{CHP}$ | Lower/upper output limits of CHP unit $j$ |
| $\overline{h}_{ij}^P$ / $\overline{S}_{ij}$ | Upper limit of pipe/line $(i,j)$ |
| $\underline{h}_j^{EB}$ / $\overline{h}_j^{EB}$ | Lower/upper limits of the heating output of EB $j$ |
| $\underline{h}_j^{HB}$ / $\overline{h}_j^{HB}$ | Lower/upper limits of the heating output of HB $j$ |
| $\underline{p}_j^{CHP}$ / $\overline{p}_j^{CHP}$ | Lower/upper limits of power output of the CHP unit $j$ |
| $\underline{p}_j^{EB}$ / $\overline{p}_j^{EB}$ | Lower/upper limits of power output of EB $j$ |
| $\underline{p}_j^{DG}$ / $\overline{p}_j^{DG}$ | Lower/upper limits of power output of DG $j$ |
| $a_j$ / $b_j$ | Weight of the electric/heating load at node/bus $j$ |
| $c_h$ / $m_{ij}$ | Specific heat capacity of water and mass flow rate in pipe $(i,j)$ |
| $\tau_{ij}^S$ / $\tau_{ij}^R$ | Water temperature of supply/return pipe |
| $\sigma$ | Penalty term coefficient |

### C. Variables

| | |
|---|---|
| $x_{m,n,c}^{crew}$ / $y_{s,c}^{crew}$ | Boolean variable that demonstrates whether maintenance crew c travels from damaged components $m$ to $n$ |
| $y_{s,c}^{crew}$ | Boolean variable demonstrates whether the damaged component $s$ is overhauled by the maintenance crew $c$ |

This work was supported by the National Natural Science Foundation of China (NSFC) under Grant U22A6007, U2066206, 52307131 and Young Elite Scientists Sponsorship Program by CSEE. (Corresponding authors: Yixun Xue; Xinyue Chang).

Ke Wang, Yixun Xue, Xinyue Chang, Zening Li, and Hongbin Sun are with Key Laboratory of Cleaner Intelligent Control on Coal & Electricity, Ministry of Education, Taiyuan University of Technology, China. (e-mail: WangK50@cardiff.ac.uk, xueyixun@tyut.edu.cn, shb@tsinghua.edu.cn)

Ke Wang and Yue Zhou are with the School of Engineering, Cardiff University, UK.

Hongbin Sun is with the Department of Electrical Engineering, Tsinghua University, China.

Mohammad Shahidehpour is with Galvin Center for Electricity Innovation, Illinois Institute of Technology, Chicago, IL, USA (e-mail: ms@iit.edu ).

| | |
|---|---|
| $AT_{s,c}^{crew}$ | Arriving time of maintainer $c$ arrives at damaged component $s$ |
| $\tau_{s,t}^{crew}$ / $c_{s,t}$ | Boolean variable indicates whether the damaged component $s$ is repaired and the status of the damaged component $s$ at time $t$ |
| $p_{j,t}$ / $q_{j,t}$ | Power injection at bus $j$ at time $t$ |
| $p_{ij,t}$ / $q_{ij,t}$ | Power flow of line $(i,j)$ at time $t$ |
| $h_{j,t}^{HS}$ / $h_{j,t}^{CHP}$ | Heating production of heat station $j$ and CHP unit $j$ at time $t$ |
| $h_{j,t}^{HB}$ / $f_{j,t}^{HB}$ | Heating production and fuel consumption of HB $j$ at time $t$ |
| $z_{ij,t}$ / $a_{ij,t}$ | Boolean variable of the status of the pipe/line $(i,j)$ and represents whether the virtual flow is flowing from $i$ to $j$ at time $t$ |
| $rt_{s,c}^{crew}$ / $tt_{s,n,c}^{crew}$ | Maintenance time for the damaged component $s$ repaired by the maintenance crew $c$ and travel time from damaged components $s$ to $n$ |
| $m_{j,t}$ / $\varsigma_{j,t}$ | Boolean variable indicates whether bus/node $j$ is located in the faulty area and whether heat/electric load at node/bus $j$ is fully recovered at time $t$ |
| $h_{j,t}^{EB}$ / $p_{j,t}^{EB}$ | Heating production and electricity consumption of EB $j$ at time $t$ |
| $p_{j,t}^{CHP}$ / $p_{j,t}^{DG}$ | Power generation of the CHP unit $j$, and DG $j$ at time $t$ |
| $h_{ij,t}^{P,out}$ / $h_{ij,t}^{P,in}$ | Outlet, and inlet heat quantities of pipe $(i,j)$ at time $t$ |
| $h_{ij,t}^{loss}$ | Heat quantity loss of pipe $(i,j)$ at time $t$ |
| $h_{j,t}^{Loss}$ / $p_{j,t}^{Loss}$ | Load shedding of node/bus $j$ at time $t$ |

## I. Introduction

In recent years, the frequency and intensity of natural disasters such as blizzards, and ice storms have significantly increased [1]. Large-scale energy interruption can occur when extreme natural disasters affect vital energy transmission equipment, including electricity cables, transmission lines, gas pipes and heat pipes [2]. In the US, the Great Texas Freeze caused heating pipes to burst and power lines to break. The energy interruption deprived approximately 4.5 million customers of heating and power, and the estimated economic loss was up to $1 billion [3]. In Jilin, China, ice disasters caused approximately 300 million individuals to experience power and heat shortages when major thermal power plants were shut down by iced transmission line galloping [4].

As the aforementioned threats proliferate, the fault recovery of energy systems in the aftermath of disasters has drawn significant attention, especially in electricity systems. Post-disaster load recovery typically involves stages of isolating faults and reinstating services [5]. During the fault isolation phase, specific fault zones are accurately pinpointed, which identifies the overhauling lines and operating switches for load restoration. In [6], a remediation strategy is implemented with the objective of identifying fault areas with loops, taking into account the topological alterations resulting from the execution of different switch operations within the electricity system. During the service restoration stage, it is necessary to timely dispatch maintenance crews to repair faulted lines to ensure the reliable operation of energy infrastructures [7]. In [8] and [9], the maintenance crew, who repairs damaged components and operates manual switches, is jointly dispatched to achieve the optimal power distribution system (PDS) restoration. In [10], a repair crew dispatch model is developed for optimal energy allocation during load restoration.

Other researchers have examined resilience-oriented restoration strategies for integrated energy systems [11]-[12]. In the fault isolation stage, a model is developed to identify susceptible elements and ensure the reliable operation of integrated electricity and natural gas systems in the presence of numerous communication interruptions [13]. In the service restoration stage, repair crews are optimally dispatched to maximize the repair efforts for a reliable energy supply. In [14], energy conversion and storage facilities are modeled, which could modify the energy distribution to meet unmet demands in multi-energy networks. In [15], a model is proposed for fault recovery in electricity and natural gas networks, which considers network reconfiguration in the PDS and the complicated relation between the PDS and the natural gas system. In [16], the dispatch of maintenance crews in the power system and natural gas systems are both dispatched to ensure resilient operation after extreme disasters.

The extensive deployment of combined heat and power (CHP) units has served to reinforce the interrelationship between the power distribution system (PDS) and the district heating system (DHS). In northern China, CHP units have met more than 45% of the heating demand [17]. The intricate interconnectivity of the PDS and DHS presents significant challenges to achieving resilient recovery in integrated electric and heating systems (IEHSs) [18]-[19]. On one hand, failures in the PDS or DHS can spread to each other, so reasonable fault isolation cannot be individually performed by PDS or DHS operators [20]-[21]. For example, improper PDS switching operation can impact the heat generation of coupling devices in the DHS and cause unnecessary load loss. On the other hand, during service restoration, independent maintenance only focuses on the timely maintenance of faults in subsystems, i.e., the PDS and DHS, to restore the energy infrastructure operation. Independent maintenance can mis-dispatch the maintenance crew at the IEHS coupling border, which can cause a long energy interruption for important electric and heat loads. For example, to reduce the time cost, the crew would not prioritize the maintenance of CHP units that are far away. This selection may prolong energy interruption due to the delayed maintenance of CHP units that work as the main energy sources and have great operational flexibility. Thus, coordinated load restoration, especially coordinated maintenance, is urgently required to increase the ability of an IEHS to withstand disasters.

The DHS reconfiguration is an important strategy for resilience-oriented restoration [22]-[23]. Similar to that of PDS, DHS reconfiguration can be achieved by the remote operation

of ties and sectionalizing valves [24]. In accordance with the design guidelines for DHS, both ties and sectionalizing valves can be utilized for the fault recovery, which can fully explore the potential flexibility of DHS reconfiguration.

Additionally, the network configuration in the DHS can be adjusted to work in conjunction with the PDS switching operation. This adjustment will prevent excessive load reductions and halt additional fault spread between PDS and DHS. In essence, the coordinated reconfiguration of PDS and DHS can explore the flexibility of a time-varying topology for complete load restoration.

This paper aims to propose a coordinated maintenance crew dispatch method for PDS/DHS operations that considers the optimal reconfiguration of coordinated networks to achieve resilience-oriented restoration. The contributions of this paper are as follows:

1) The DHS and PDS maintenance crews in the multiperiod coordinated recovery model (MCRM) are coordinated for restoration. Considering the intricate mutual interactions between subsystems, coordinated maintenance can redesign the optimal maintenance sequence for crucial energy infrastructures, which can ensure that essential electric and heating demands receive prompt energy deliveries.
2) A coordinated reconfiguration is employed to investigate the flexibility of time-varying topologies for fault recovery. The network architecture of the DHS is modified in synchrony with the PDS switching processes, thus effectively minimizing excessive load reductions and preventing significant fault propagation across the networks.
3) A two-stage acceleration algorithm is proposed for fast decision-making in the proposed MCRM, which divides the solution procedure into two stages according to the types of integer variables and analyzes the acceleration principles for determining load status variables.

The subsequent sections are structured as follows: Section II describes a park-level IEHS and the mutual impacts between subsystems after disasters in detail. Section III formulates an MCRM, which describes the spread of faults across subsystems, and the coordinated maintenance and reconfiguration models. Section IV proposes a two-stage acceleration algorithm for the fast decision-making of the problem. Section V presents the outcomes for the two test systems. Section VI outlines the conclusions and suggestions for future works.

## II. MCRM Problem Description

A park-level IEHS (Fig. 1) typically consists of PDS and DHS subsystems that are closely linked by coupling components such as small CHP units and electric boilers (EBs). To improve the ability of the IEHS to handle major disasters, we optimize the coordinated PDS and DHS maintenance for damaged components, which considers the intricate interactions between the two subsystems. Furthermore, the reconfiguration of the PDS and DHS is synchronized for resilient restoration. This step involves changing the DHS network architecture in conjunction with switch operations in the PDS.

To elucidate the mutual impacts among subsystems and ensure the prompt delivery of energy to essential loads, a restoration approach is proposed, which integrates the stages of fault isolation and service restoration. During the fault isolation stage, the operators of the PDS and DHS subsystems collaborate to identify faulted areas and describe the fault propagations between the two subsystems. During the fault recovery stage, coordinated maintenance and reconfiguration are fully utilized to achieve resilient restoration in the IEHS.

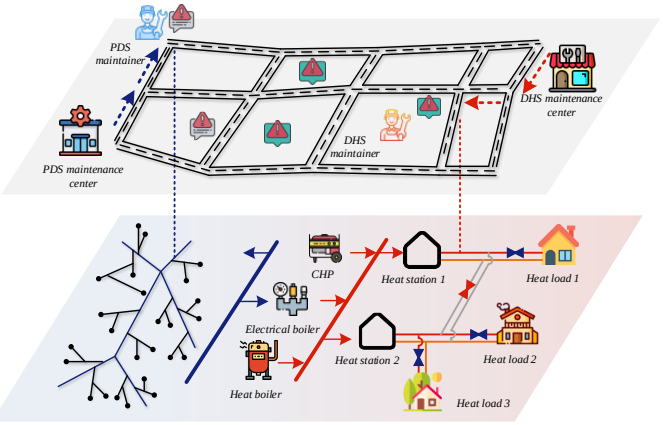


**Fig. 1.** Framework of coordinated maintenance scheduling in park-level IEHS.

## III. MCRM Formulation

The proposed MCRM is formulated in this section, which aims to determine the optimal network topologies and travel paths for maintenance crews. The MCRM encompasses stages of fault isolation and service restoration. It depicts fault spread among subsystems during the isolation stage and analyses the effects of synchronized maintenance with network restructuring during the restoration stage.

### A. Coordinated Maintenance Constraint of PDS and DHS

Coordinated maintenance constraints are established based on the vehicle-routing problem [25]. The damaged pipes/lines are respectively repaired by the PDS/DHS maintenance crew, where the corresponding travel paths are coordinated considering the interactions between subsystems. The coordinated maintenance constraints of the PDS and DHS are formulated as follows.

#### 1) PDS/DHS Maintenance Crew Dispatch Constraints

$$\sum_{s\in k^{FP}\bigcup k^{FL}} x_{0,s,c}^{crew} - \sum_{s\in k^{FP}\bigcup k^{FL}} x_{s,0,c}^{crew} = 1, \forall c, \tag{1}$$

$$\sum_{s\in k^{FP}\bigcup k^{FL}} x_{end,s,c}^{crew} - \sum_{s\in k^{FP}\bigcup k^{FL}} x_{s,end,c}^{crew} = -1, \forall c, \tag{2}$$

where “0” and “end” both indicate the maintenance center in the PDS/DHS. $x_{0,s,c}^{crew}$ and $x_{end,s,c}^{crew}$ indicate whether the crew $c$ travels from the maintenance center to the damaged component $s$. $x_{s,0,c}^{crew}$ and $x_{s,end,c}^{crew}$ indicate whether the crew $c$ travels from the damaged component $s$ to the maintenance center. Constraints (1)-(2) indicate that the maintenance crew starts

from the maintenance center and must return to the center after the repair work is finished.

$$\sum_{\forall c} y_{s,c}^{crew} = 1,\ y_{s,c}^{crew} = \sum_{m \in k^{FP} \bigcup k^{FL}} x_{m,s,c}^{crew},\ \forall s \in k^{FP} \bigcup k^{FL}, \forall c, \quad (3)$$

Constraint (3) indicates that each damaged component $s$ is repaired by only one maintenance crew.

$$\sum_{m \in k^{FP} \bigcup k^{FL}} x_{m,s,c}^{crew} - \sum_{n \in k^{FP} \bigcup k^{FL}} x_{s,n,c}^{crew} = 0, \forall s \in k^{FP} \bigcup k^{FL}, \forall c, \quad (4)$$

Constraint (4) indicates that the number of maintenance crews who arrive at a damaged pipe/line is equal to the number of maintenance crews who depart since the crew must leave after the repair work has been completed.

*2) PDS/DHS Maintenance Time Constraints*

$$T_{R_0} \le AT_{s,c}^{crew} \le y_{s,c}^{crew} M, \forall s \in k^{FP} \bigcup k^{FL}, \forall c, \quad (5)$$

$$\begin{aligned} &AT_{s,c}^{crew} + rt_{s,c}^{crew} + tt_{s,n,c}^{crew} - AT_{n,c}^{crew} \le \left(1 - x_{s,n,c}^{crew}\right) M, \\ &\forall (s,n) \in k^{FP} \bigcup k^{FL}, \forall c, \end{aligned} \quad (6)$$

$$\begin{aligned} &-\left(1 - x_{s,n,c}^{crew}\right) M \le AT_{s,c}^{crew} + rt_{s,c}^{crew} + tt_{s,n,c}^{crew} - AT_{n,c}^{crew}, \\ &\forall (s,n) \in k^{FP} \bigcup k^{FL}, \forall c, \end{aligned} \quad (7)$$

where $T_{R_0}$ indicates the start time of service restoration. Constraint (5) indicates that all maintenance crews immediately start from the maintenance center in the service restoration stage and the arrival time is $T_{R_0}$ when the maintenance crew $c$ does not arrive at the damaged component $s$. Constraints (6)-(7) indicates that the arrival time for the damaged component $n$ considers the travel time from $s$ to $n$ and maintenance time at $s$.

$$\sum_{\forall t} \tau_{s,t}^{crew} = 1, \forall s \in k^{FP} \bigcup k^{FL}, \forall t \in T_R, \quad (8)$$

$$\begin{aligned} &\sum_{\forall c} \left( AT_{s,c}^{crew} + rt_{s,c}^{crew} y_{s,c}^{crew} \right) \le \sum_{\forall t} t \tau_{s,c}^{crew}, \\ &\forall s \in k^{FP} \bigcup k^{FL}, \forall t \in T_R, \forall c, \end{aligned} \quad (9)$$

$$\begin{aligned} &\sum_{\forall t} t \tau_{s,t}^{crew} \le \sum_{\forall c} \left( AT_{s,c}^{crew} + rt_{s,c}^{crew} y_{s,c}^{crew} \right) + 1 - \varepsilon, \\ &\forall s \in k^{FP} \bigcup k^{FL}, \forall t \in T_R, \forall c, \end{aligned} \quad (10)$$

where $\tau_{s,t}^{crew}$ indicates whether the damaged component $s$ is repaired at $t$. Constraint (8) indicates that if the repair work has not started or finished, $\tau_{s,t}^{crew}$ is zero. Constraint (9) indicates the relation of the arrival time, maintenance time, and finishing time for the damaged component $s$.

*3) Coupling Constraints of Maintenance and Reconfiguration*

$$\begin{aligned} &c_{s,t} = \sum_{k=1}^{t-1} \tau_{s,k}^{crew},\ z_{ij,t} \le c_{s,t}, \\ &\forall s \in k^{FP} \bigcup k^{FL}, \forall (i,j) \in k^{pipe} \bigcup k^{line} \forall t \in T_R, \end{aligned} \quad (11)$$

Constraint (11) ensures that the damaged component $s$, which represents the pipe/line $(i,j)$, will restart operation and can be utilized for PDS/DHS reconfiguration once it has been repaired.

## B. PDS/DHS Network Topology Constraints

*1) PDS/DHS Fault Isolation Constraints*

Based on the PDS fault isolation model in [26], the fault isolation constraints are established considering the sophisticated coupling characteristics of the PDS and DHS, which describe the faulted region isolation and the fault propagation between DHS and PDS.

$$\begin{aligned} &z_{ij,t} \ge \left(1 - f_{ij}\right)\left(z_{ij,0} - s_{ij,0}\right), \\ &\forall (i,j) \in k^{pipe} \bigcup k^{line}, \forall s \in k^{FP} \bigcup k^{FL}, \forall t \in T_I, \end{aligned} \quad (12)$$

$$\begin{aligned} &z_{ij,t} \le \left(1 - f_{ij}\right)\left(z_{ij,0} + s_{ij,0}\right), \\ &\forall (i,j) \in k^{pipe} \bigcup k^{line}, \forall s \in k^{FP} \bigcup k^{FL}, \forall t \in T_I, \end{aligned} \quad (13)$$

$$\begin{aligned} &m_{i,t} - z_{ij,0} + 1 \ge f_{ij}\left(1 - s_{ij,0}\right), \\ &\forall (i,j) \in k^{pipe} \bigcup k^{line}, \forall s \in k^{FP} \bigcup k^{FL}, \forall t \in T_I, \end{aligned} \quad (14)$$

$$\begin{aligned} &m_{j,t} - z_{ij,0} + 1 \ge f_{ij}\left(1 - s_{ij,0}\right), \\ &\forall (i,j) \in k^{pipe} \bigcup k^{line}, \forall s \in k^{FP} \bigcup k^{FL}, \forall t \in T_I, \end{aligned} \quad (15)$$

$$m_{i,t} + z_{ij,t} - 1 \le m_{j,t}, \forall (i,j) \in k^{pipe} \bigcup k^{line}, \forall t \in T_I, \quad (16)$$

$$m_{j,t} + z_{ij,t} - 1 \le m_{i,t}, \forall (i,j) \in k^{pipe} \bigcup k^{line}, \forall t \in T_I, \quad (17)$$

$$m_{r,t} = m_{d,t}, \forall r \in k_{i,n}^{CHP} \bigcup k_{i,n}^{EB}, \forall d \in k_{i,b}^{CHP} \bigcup k_{i,b}^{EB}, \forall t \in T_I, \quad (18)$$

Constraint (12) indicates that the non-faulted pipe/line $(i,j)$ installed with a valve/switch can be switched on/off for fault isolation. Also, the damaged pipe/line $(i,j)$ must be opened for repair. Constraints (14)-(15) demonstrate that the valve/switch located on a pipe/line $(i,j)$ can position nodes/buses $i$ and $j$ in non-faulty areas. Constraints (16)-(17) indicate that the nodes/buses $i$ and $j$ of a closed pipe/line are situated within the same area. Constraint (18) illustrates that the area where the CHP unit/EB $i$ is located can be considered in both DHS and PDS analyses. For example, when the CHP unit/EB $i$ is placed in a faulted PDS region, it will be divided into the same region in the DHS.

*2) PDS/DHS Service Restoration Constraints*

At this stage, PDS/DHS reconfiguration will be conducted to implement the coordinated maintenance to ensure that the extended energy can supply both electric and heating loads. Also, the service restoration constraints consider the coupling relationship of the PDS and DHS, which are originally formulated as follows:

$$\begin{aligned} &z_{ij,t} \ge \left(1 - f_{ij} + c_{s,t}\right)\left(z_{ij,t\text{-}1} - s_{ij,0}\right), \\ &\forall (i,j) \in k^{pipe} \bigcup k^{line}, \forall s \in k^{FP} \bigcup k^{FL}, \forall t \in T_R, \end{aligned} \quad (19)$$

$$\begin{aligned} &z_{ij,t} \le \left(1 - f_{ij} + c_{s,t}\right)\left(z_{ij,t\text{-}1} + s_{ij,0}\right), \\ &\forall (i,j) \in k^{pipe} \bigcup k^{line}, \forall s \in k^{FP} \bigcup k^{FL}, \forall t \in T_R, \end{aligned} \quad (20)$$

$$\begin{aligned} &m_{i,t} - z_{ij,0} + 1 \ge \left(f_{ij} - c_{s,t}\right)\left(1 - s_{ij,0}\right), \\ &\forall (i,j) \in k^{pipe} \bigcup k^{line}, \forall s \in k^{FP} \bigcup k^{FL}, \forall t \in T_R, \end{aligned} \quad (21)$$

$$m_{j,t}-z_{ij,0}+1\geq\left(f_{ij}-c_{s,t}\right)\left(1-s_{ij,0}\right),\quad \forall(i,j)\in k^{pipe}\bigcup k^{line},\forall s\in k^{FP}\bigcup k^{FL},\forall t\in T_R, \tag{22}$$

$$m_{i,t}+z_{ij,t}-1\leq m_{j,t},\forall(i,j)\in k^{pipe}\bigcup k^{line},\forall t\in T_R, \tag{23}$$

$$m_{j,t}+z_{ij,t}-1\leq m_{i,t},\forall(i,j)\in k^{pipe}\bigcup k^{line},\forall t\in T_R, \tag{24}$$

$$m_{r,t}=m_{d,t},\forall r\in k_{i,n}^{CHP}\bigcup k_{i,n}^{EB},\forall d\in k_{i,b}^{CHP}\bigcup k_{i,b}^{EB},\forall t\in T_R, \tag{25}$$

Constraints (19)-(20) indicate that the component $s$ in the damaged pipe/line $(i,j)$ will be considered disconnected before the pipe/line $(i,j)$ is repaired. Also, repaired or non-faulted pipe/line $(i,j)$ with a valve/switch can be switched on or off for load restoration. Constraints (21)-(22) illustrate that the valve/switch on restored or intact pipe/line can place linked nodes/buses in non-faulted regions. Constraints (23)-(24) illustrate that nodes/buses linked by a closed pipe/line must be situated together. Constraint (25) illustrates that DHS and PDS analyses consider the belonged area of CHP unit/EB $i$.

$$\sum_{\forall(i,j)\in k^{pipe}\bigcup k^{line}} z_{ij,t}=N_A-N_S, \tag{26}$$

$$\sum_{i\in\pi(j)} a_{ij,t}=0,j\in\Omega^E\bigcup\Omega^H,\forall t\in T_R, \tag{27}$$

$$\sum_{i\in\pi(j)} a_{ij,t}\leq 1,j\in\left(k^{node}\setminus\Omega^H\right)\bigcup\left(k^{bus}\setminus\Omega^E\right),\forall t\in T_R, \tag{28}$$

$$z_{ij,t}=a_{ij,t}+a_{ji,t},\forall(i,j)\in k^{pipe}\bigcup k^{line},\forall t\in T_R, \tag{29}$$

where $N_A$ and $N_S$ represent the number of nodes/buses and root nodes/buses, respectively. The network topology of the PDS/DHS should be radial [27]. Constraint (26) shows a necessary condition for the radial PDS/DHS topology. Constraint (27) implies that the power/heat station does not have a parent bus/node. Constraint (28) illustrates that each bus/node can have at most one parent bus/node. Constraint (29) illustrates the relation between the status and virtual flow of pipe/line $(i,j)$. Constraints (27)-(29) present a sufficient condition for the radial PDS/DHS topology [28]-[29].

### C. PDS/DHS Operation Constraints

#### 1) DHS Operation Constraints

The precise DHS model is a complex mixed-integer nonlinear problem, which introduces challenges when addressing the multiperiod restoration problem [30]. We introduce a decision variable, denoted as $h_{ij}=c_h m_{ij}\left(\tau_{ij}^S-\tau_{ij}^R\right)$, to represent the heat quantity in pipes, and apply the energy flow model to solve the proposed MCRM. Thus, the DHS operation constraints are expressed as follows.

$$\underline{\nu}_j h_{j,t}^{CHP}\leq p_{j,t}^{CHP}\leq\overline{\nu}_j h_{j,t}^{CHP},\forall\ j\in k^{CHP},\forall t\in T, \tag{30}$$

$$p_{j,t}^{EB}=\sigma_j h_{j,t}^{EB},\forall\ j\in k^{EB},\forall t\in T, \tag{31}$$

$$h_{j,t}^{HB}=\gamma_j f_{j,t}^{HB},\forall\ j\in k^{HB},\forall t\in T, \tag{32}$$

$$\sum_{j\in k_k^{CHP}} h_{j,t}^{CHP}+\sum_{j\in k_k^{HB}} h_{j,t}^{HB}+\sum_{j\in k_k^{EB}} h_{j,t}^{EB}=h_{k,t}^{HS},\forall k\in k^{HS},\forall t\in T, \tag{33}$$

$$\sum_{(j,s)\in S_j^{pipe-}} h_{js,t}^{P,out}+\sum_{k\in k_j^{HS}} h_{k,t}^{HS}=h_{j,t}^{L}-h_{j,t}^{Loss}+\sum_{(i,j)\in S_j^{pipe+}} h_{ij,t}^{P,in},\quad \forall j\in k^{nd},\forall t\in T, \tag{34}$$

Constraint (30) illustrates that the power generation of CHP unit $j$ is influenced by the heat generation. Constraint (31) indicates that the power consumption of EB $j$ is correlated with the heat generation. Constraint (31) illustrates that the heat generation of heating boiler (HB) $j$ is determined by the fuel consumption. Constraint (33) indicates that the total heat produced at the station $k$ encompasses contributions from the installed CHP unit, EB, and HB. Constraint (34) describes a detailed account of the energy equilibrium at node $j$.

$$h_{ij,t}^{P,out}=h_{ij,t}^{P,in}-h_{ij,t}^{loss},\forall\left(i,j\right)\in k^{pipe},\forall t\in T, \tag{35}$$

$$-z_{ij,c,t}\overline{h}_{ij}^{P}\leq h_{ij,c,t}^{P,in}\leq z_{ij,c,t}\overline{h}_{ij}^{P},\forall\left(i,j\right)\in k^{pipe},\forall t\in T, \tag{36}$$

$$-z_{ij,c,t}\overline{h}_{ij}^{P}\leq h_{ij,c,t}^{P,out}\leq z_{ij,c,t}\overline{h}_{ij}^{P},\forall\left(i,j\right)\in k^{pipe},\forall t\in T, \tag{37}$$

Constraint (35) illustrates the heat loss between the outlet and the inlet of pipe $(i,j)$. Constraints (36)-(37) illustrate the heat quantity limitations of pipe $(i,j)$.

$$\left(1-m_{j,t}\right)\underline{h}_j^{CHP}\leq h_{j,t}^{CHP}\leq\left(1-m_{j,t}\right)\overline{h}_j^{CHP},\forall j\in k^{CHP},\forall t\in T, \tag{38}$$

$$\left(1-m_{j,t}\right)\underline{h}_j^{EB}\leq h_{j,t}^{EB}\leq\left(1-m_{j,t}\right)\overline{h}_j^{EB},\forall j\in k^{EB},\forall t\in T, \tag{39}$$

$$\left(1-m_{j,t}\right)\underline{h}_j^{HB}\leq h_{j,t}^{HB}\leq\left(1-m_{j,t}\right)\overline{h}_j^{HB},\forall j\in k^{HB},\forall t\in T, \tag{40}$$

Constraint (39)-(40) illustrates that the heat generation of heat sources in the faulted and non-faulted area, including the CHP unit, EB, and HB.

$$h_{j,t}^{Loss}=\varsigma_{j,t}h_{j,t}^{L},m_{j,t}h_{j,t}^{L}\leq h_{j,t}^{Loss}\leq h_{j,t}^{L},\forall j\in k^{nd},\forall t\in T, \tag{41}$$

Constraint (41) illustrates that all loads are lost in the faulted area and the heating loads can be shed in the non-faulted area for energy balance.

#### 2) PDS Operation Constraints

The PDS operation constraints are established based on second-order cone relaxation (SOCR), which is a typical relaxation method for the original Distflow model [31]. Based on the assumption that the three-phase power distribution system is approximately balanced [32], the power flow model based on the SOCR relaxation is widely used in research for load restoration in PDS and integrated energy systems, demonstrating its effectiveness in optimizing and managing power flow during recovery processes [33]-[34]. The multiperiod coordinated restoration problem is formulated as a mixed-integer second-order cone problem (MISOCP).

$$p_{j,t}=\sum_{s\in\delta(j)} p_{js,t}-\sum_{i\in\pi(j)}\left(p_{ij,t}-r_{ij}l_{ij,t}\right),\forall j\in k^{bus},\forall t\in T, \tag{42}$$

$$q_{j,t}=\sum_{s\in\delta(j)} q_{js,t}-\sum_{i\in\pi(j)}\left(q_{ij,t}-x_{ij}l_{ij,t}\right),\forall j\in k^{bus},\forall t\in T, \tag{43}$$

$$p_{j,t}=p_{j,t}^{DG}+p_{j,t}^{CHP}-p_{j,t}^{EB}-\left(p_j^L-p_{j,t}^{Loss}\right),\forall j\in k^{bus},\forall t\in T, \tag{44}$$

$$q_{j,t}=q_{j,t}^{DG}+q_{j,t}^{CHP}-q_{j,t}^{EB}-\left(q_j^L-q_{j,t}^{Loss}\right),\forall j\in k^{bus},\forall t\in T, \tag{45}$$

$$\left\|2p_{ij,t}\ \ 2q_{ij,t}\ \ l_{ij,t}-u_{i,t}\right\|_2\leq l_{ij,t}+u_{i,t},\forall j\in k^{bus},\forall t\in T, \tag{46}$$

$$-z_{ij,t}\overline{S}_{ij}\leq p_{ij,t}\leq z_{ij,t}\overline{S}_{ij},\forall(i,j)\in k^{line},\forall t\in T, \tag{47}$$

$$-z_{ij,t}\overline{S}_{ij} \le q_{ij,t} \le z_{ij,t}\overline{S}_{ij}, \forall (i,j) \in k^{line}, \forall t \in T, \quad (48)$$

Constraints (42)-(43) illustrate the power injection into bus $j$. Constraints (44)-(45) illustrate the power equilibrium at bus $j$. Constraint (46) illustrates the power flow equation of line $(i,j)$ after second-order cone relaxation. Constraints (47)-(48) illustrate the transmission limit of line $(i,j)$.

$$u_{i,t} - u_{j,t} - 2\left(r_{ij}p_{ij,t} + x_{ij}q_{ij,t}\right) + \left(r_{ij}^2 + x_{ij}^2\right)l_{ij,t} \le \left(1 - z_{ij,t}\right)M, \quad (49)$$
$$\forall (i,j) \in k^{line}, \forall t \in T,$$

$$u_{i,t} - u_{j,t} - 2\left(r_{ij}p_{ij,t} + x_{ij}q_{ij,t}\right) + \left(r_{ij}^2 + x_{ij}^2\right)l_{ij,t} \ge -\left(1 - z_{ij,t}\right)M, \quad (50)$$
$$\forall (i,j) \in k^{line}, \forall t \in T,$$

$$\underline{u}_j \le u_{j,t} \le \overline{u}_j, \forall j \in k^{bus}, \forall t \in T, \quad (51)$$

Constraints (49)-(50) illustrate the voltage drop along a closed line $(i,j)$. Also, the voltages of bus $i$ and $j$ do not impact each other when line $(i,j)$ is open. Constraint (51) illustrates the voltage limitation of bus $j$.

$$\left(1 - m_{j,t}\right)\underline{p}_j^{CHP} \le p_{j,t}^{CHP} \le \left(1 - m_{j,t}\right)\overline{p}_j^{CHP}, \forall j \in k^{CHP}, \forall t \in T, \quad (52)$$

$$\left(1 - m_{j,t}\right)\underline{q}_j^{CHP} \le q_{j,t}^{CHP} \le \left(1 - m_{j,t}\right)\overline{q}_j^{CHP}, \forall j \in k^{CHP}, \forall t \in T, \quad (53)$$

$$\left(1 - m_{j,t}\right)\underline{p}_j^{DG} \le p_{j,t}^{DG} \le \left(1 - m_{j,t}\right)\overline{p}_j^{DG}, \forall j \in k^{DG}, \forall t \in T, \quad (54)$$

$$\left(1 - m_{j,t}\right)\underline{q}_j^{DG} \le q_{j,t}^{DG} \le \left(1 - m_{j,t}\right)\overline{q}_j^{DG}, \forall j \in k^{DG}, \forall t \in T, \quad (55)$$

Constraints (52)-(55) illustrate the power source generation, including those of the CHP unit $j$ and DG $j$, in a faulted/non-faulted area. For example, if the CHP unit $j$ is shut down in the faulted area, its power generation will be reduced to zero. The power generation of the CHP unit $j$ in the non-faulted area is constrained within its stated range.

$$p_{j,t}^{Loss} = \varsigma_{j,t}, p_j^L, \forall j \in k^{bus}, \forall t \in T, \quad (56)$$

$$q_{j,t}^{Loss} = \varsigma_{j,t} q_j^L, \forall j \in k^{bus}, \forall t \in T, \quad (57)$$

$$m_{j,t}p_j^L \le p_{j,t}^{Loss} \le p_j^L, \ \forall j \in k^{bus}, \forall t \in T, \quad (58)$$

$$m_{j,t}q_j^L \le q_{j,t}^{Loss} \le q_j^L, \ \forall j \in k^{bus}, \forall t \in T, \quad (59)$$

Constraints (56)-(59) illustrate the loads in the faulted and non-faulted areas.

### *D. MCRM Objective and Resilience Metrics*

To optimize the recovery of electrical and thermal loads over multiple periods, the objective of (60) is proposed, to ensure that essential loads promptly receive energy. The third element involves a network loss penalty to maintain the precision of the MCRM following the SOCR, which must remain minimal. The resilience metrics proposed in (63) reflect the proportion of load restoration throughout the recovery phase.

$$\max f(\varsigma) = \Delta T_I L_I^{Res} + \Delta T_R L_R^{Res} - \sigma \sum_{\forall t} p_t^{Nloss} \quad (60)$$

$$L_I^{Res} = \sum_{\forall j} a_j \left(1 - \varsigma_{j,t_I}^e\right) + \sum_{\forall j} b_j \left(1 - \varsigma_{j,t_I}^h\right),$$
$$L_R^{Res} = \sum_{\forall t_R}\sum_{\forall j} a_j \left(1 - \varsigma_{j,t_R}^e\right) + \sum_{\forall t_R}\sum_{\forall j} b_j \left(1 - \varsigma_{j,t_R}^h\right), \quad (61)$$

$$R = 1 - \frac{\Delta T_I L_I^{Loss} + \Delta T_R L_R^{Loss}}{\Delta T_I \left(\sum_{\forall j}\left(a_j + b_j\right)\right) + \Delta T_R \left(\sum_{\forall t_R}\sum_{\forall j}\left(a_j + b_j\right)\right)}, \quad (62)$$

$$L_I^{Loss} = \sum_{\forall j} a_j \varsigma_{j,t_I}^e + \sum_{\forall j} b_j \varsigma_{j,t_I}^e,$$
$$L_R^{Loss} = \sum_{\forall t_R}\sum_{\forall j} a_j \varsigma_{j,t_R}^e + \sum_{\forall t_R}\sum_{\forall j} b_j \varsigma_{j,t_R}^e \Delta T_R. \quad (63)$$

Fig. 2 shows the flowchart of the proposed model to better illustrate the MCRM formulation. During the fault isolation stage, the variables include the PDS/DHS network topology variables in this stage and the PDS/DHS operation variables. During the service restoration stage, the variables include the coordinated maintenance variables of the PDS and DHS, PDS/DHS network topology variables in this stage and PDS/DHS operation variables.

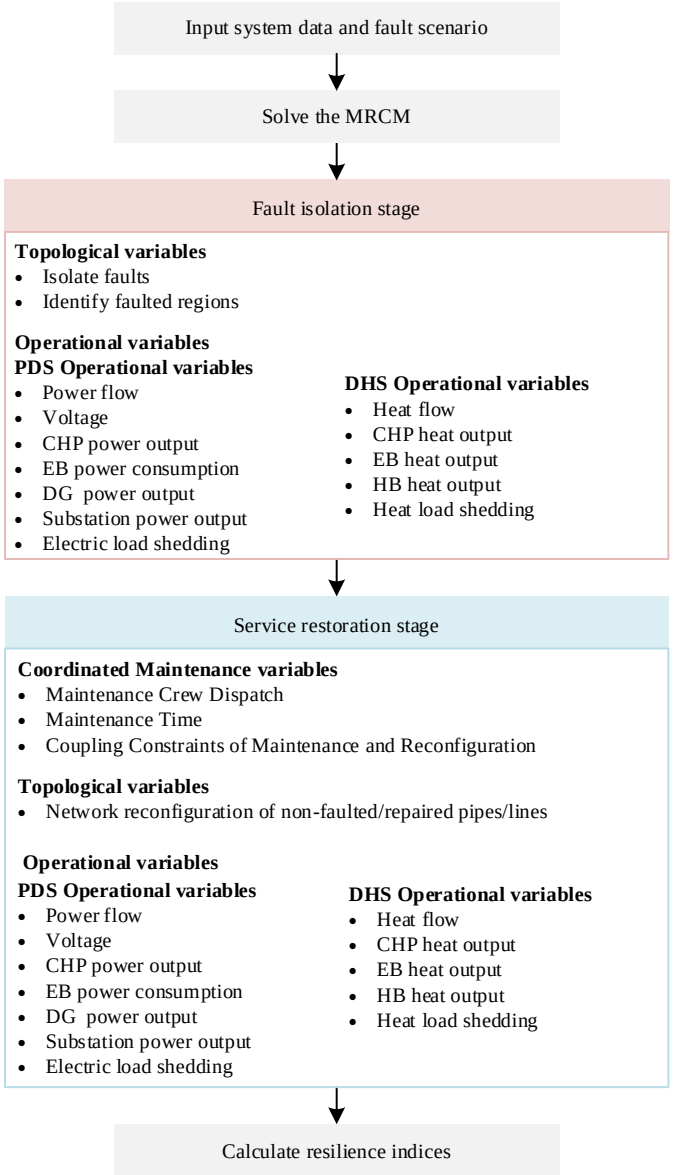


**Fig. 2.** The flowchart of MCRM.

## IV. Proposed MCRM Solution Procedure

The proposed MCRM contains many integer variables representing load statuses, travel routes for PDS/DHS maintenance crews, and PDS/DHS network topologies, which can lead to slow convergence and excessive solution time [35]. To reduce the computational complexity, we propose a two-stage acceleration algorithm (TSAA) in this section to balance computation accuracy and efficiency, which is suitable for fast decision-making in the load restoration problem.

### A. MCRM in Compact Form

The multiperiod coordinated restoration model is presented concisely as a matrix expression.

$$\text{MCRM:}\ \max\ f(\varsigma) \tag{64}$$

$$s.t.\quad \mathbf{I}(\mathbf{y},\varsigma,\mathbf{c})\geq 0,\quad \mathbf{E}(\mathbf{y},\varsigma,\mathbf{c})=0,\quad \mathbf{y},\varsigma\in\{0,1\},\quad \mathbf{c}\in[\mathbf{c}_{\min},\mathbf{c}_{\max}] \tag{65}$$

where the integer variable vector $\varsigma$ denotes the load status variables. The integer variable vector $\mathbf{y}$ excludes the aforementioned variables. The vector of continuous variables $c$ is defined. The $\mathbf{I}(\mathbf{y},\varsigma,\mathbf{c})\geq 0$ and $\mathbf{E}(\mathbf{y},\varsigma,\mathbf{c})=0$ are defined as inequality and equality constraints, , respectively.

### B. Two-stage Acceleration Algorithm for MCRM

To deal with the integer variables in MCRM, a two-stage acceleration algorithm is proposed as follows:

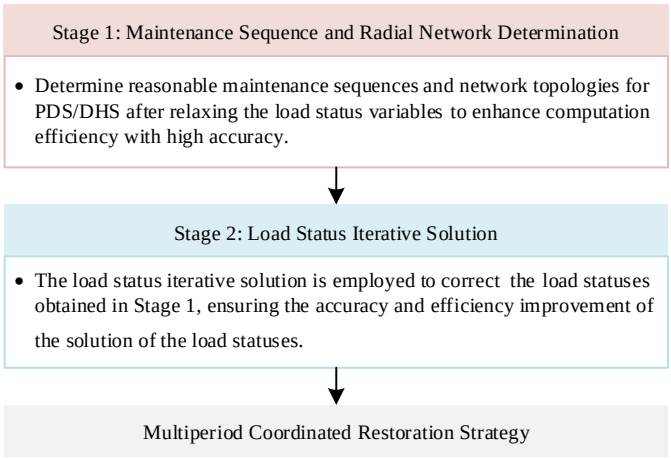


**Fig. 3.** The two-stage acceleration algorithm framework for MCRM.

The integer variables in MCRM are divided into two types, i.e., load status variables, and variables associated with travel routes for maintenance crews and network topologies of the PDS and DHS.

In Stage 1, we determine reasonable maintenance sequences and network topologies for the PDS/DHS after relaxing the load status variables. The original MCRM is transformed into a more tractable problem under relaxed constraints, which approximates the optimal solution. In Stage 2, we adjust the solution of the load statuses. The load status iterative solution is used to correct or improve the load statuses obtained in Stage 1 to ensure the accuracy and efficiency improvement of the solution of the load statuses. The problem is formulated as an SOCP. The load status iterative solution is used based on the results established in Stage 1 to determine the load status according to the proposed acceleration principles.

It is worth noting that the solution of the MCRM in Stage 2 can be infeasible when the energy balance of the coupling units cannot be satisfied with the new restrictions. Thus, we modify the additional constraints by removing the extra load restorations from small to large, which are connected to the coupling elements.

| Acceleration Algorithm for the Two-stage MCRM | |
|---|---|
| 1 | Determine the maintenance sequences and network topologies of PDS and DHS based on MCRM-MISOCP |
| 2 | Establish MCRM-SOCP based on the determined maintenance sequences and topologies and solve the MCRM-SOCP model |
| 3 | $\varsigma^{*}\leftarrow\varsigma$ solved by MCRM-SOCP |
| 4 | **while** $\varsigma^{*}$ contains non-integer values |
| 5 | Execute **function A** in PDS and DHS respectively and add constraints. Solve the MCRM-SOCP model with new constraints |
| 6 | **if** the model with new constraints can be solved |
| 7 | $\varsigma^{*}\leftarrow$solution $\varsigma$ of updated MCRM-SOCP |
| 8 | **else** |
| 9 | Compare load restorations connected to the coupling elements and remove the extra load restorations from small to large |
| 10 | **end** |
| 11 | **end while** |
| 12 | Based on this $\varsigma^{*}$, solve the energy flow with the minimum network loss as the objective |
| 13 | **return** the solution $\varsigma^{*}$ and energy flow |

#### 1) Maintenance Sequence and Radial Network Determination

The MCRM-MISOCP is formulated in (66) and (67) in stage 1, where $\varsigma$ is relaxed to be a vector of continuous variables. Notably, the load status variables are relaxed to enhance the computational speed with high accuracy.

$$\text{MCRM - MISOCP: max}\ f(\varsigma) \tag{66}$$

$$s.t.\quad \mathbf{I}(\mathbf{y},\varsigma,\mathbf{c})\geq 0,\quad \mathbf{E}(\mathbf{y},\varsigma,\mathbf{c})=0,\quad \mathbf{y}\in\{0,1\},\ 0\leq\varsigma\leq 1,\quad \mathbf{c}\in[\mathbf{c}_{\min},\mathbf{c}_{\max}] \tag{67}$$

After solving the MCRM-MISOCP, we determine a reasonable PDS/DHS maintenance sequence and a radial topology. Most load statuses are integers, and there are few non-integer values. The main reasons are summarized as follows: the load weights are included in the objective function, and the load weights $a_{k_1}>\sum_{j\in\Upsilon^{k_2}}a_j$, $b_{k_1}>\sum_{j\in\Upsilon^{k_2}}b_j$ are satisfied when the load level $k_1<k_2$, where $\Upsilon^{k_2}$ indicates that the load set that load level is $k_2$. Thus, the important loads have much larger weights than other loads, and important loads that satisfy all constraints can be fully restored; ii) the objective function ensures the smallest network loss, and the determined recovered load statuses should be the optimal solutions; iii) only a few loads are partially recovered when the capacities of the energy sources, branch current, heat quantity of the pipe, and node voltage are limited, i.e., the load statuses are non-integer values. Thus, the original MCRM is transformed into a more tractable problem after $\varsigma$ has been relaxed to become a vector of continuous variables. The optimal solution is approximated,

and the MCRM-MISOCP can enhance the computational efficiency without significantly compromising the accuracy.

*2) Load Status Iterative Solution*

After determining the PDS/DHS maintenance sequences and topologies, we solve the MCRM-SOCP stated in (68) and (69), execute function A in the PDS/DHS, and add new constraints. We remove the extra load restorations connected to the coupling elements from small to large to guarantee the energy balance of the coupling units. Fig. 4 shows the flowchart of function A in the PDS and DHS.

$$\text{MCRM-SOCP}: \max \ f(\varsigma) \tag{68}$$

$$s.t. \quad \mathbf{I}(\mathbf{y},\varsigma,\mathbf{c}) \geq 0, \quad \mathbf{E}(\mathbf{y},\varsigma,\mathbf{c}) = 0, \quad \mathbf{y} = \mathbf{y}^*, \ 0 \leq \varsigma \leq 1, \quad \mathbf{c} \in [\mathbf{c}_{\min}, \mathbf{c}_{\max}] \tag{69}$$

where $\mathbf{y}^*$ is the vector of the binary variables determined by the MCRM-MISOCP solution in Stage 1.

We analyze the acceleration principles for determining the load status variables in PDS/DHS that can be rapidly processed and introduce three corresponding load sets, i.e., $\Upsilon_{L1}, \Upsilon_{L2}, \Upsilon_{L3}$, as shown in Fig. 4. The three acceleration principles of the PDS/DHS load status are described in detail as follows:

i) If $\Upsilon_{L1} \neq \varnothing$, we add the constraint $\varsigma_j = 1, j \in \Upsilon_{L1}$. For detailed analysis, we take the acceleration principle for electric loads as an example. With appropriate generality, the inequality constraint (70) will be formulated in each iteration.

$$f(\varsigma) \leq f^{e*}_{MCRM} \leq f^{e*}_{MCRM\text{-}SOCP}, \tag{70}$$

where $f^{e*}_{MCRM\text{-}SOCP}$ and $f^{e*}_{MCRM}$ denote the optimal values of electric load restoration in the MCRM-SOCP and MCRM. $f(\varsigma)$ denotes the optimal values in each iteration.

The reason for adding the constraint is that if any load in $\Upsilon^e_{L1}$ is restored, the inequality (71) will be formulated based on the identification of the load level and sets in Fig. 4, i.e., $w^{K^{e*}-1} > f^{e*}_{MCRM\text{-}SOCP} - f^{e}_{\varsigma_j=0}$. This conflicts with inequality (70). Therefore, loads $\Upsilon^e_{L1}$ cannot be recovered.

$$f(\varsigma) = f^{e}_{\varsigma_j=0} + w^e_j \geq f^{e}_{\varsigma_j=0} + w^{K^{e*}-1} > f^{e*}_{MCRM\text{-}SOCP}, \tag{71}$$

where $w^e_j$ is the load level of load $j$ in $\Upsilon_{L1}$, $f^{e}_{\varsigma_j=0}$ denotes the value of the electric load restoration after modifying the non-integer electric load status into 1.

ii) If $\Upsilon_{L1} = \varnothing$ and $\Upsilon_{L2} \neq \varnothing$, we increase the constraint $\varsigma_j = 1$ for the load with the largest load status value in $\Upsilon_{L2}$. The reason is that if all loads in $\Upsilon_{L2}$ are restored, the node voltage, branch current, or heat quantity of the pipe will exceed the limit. Therefore, at least one load in $\Upsilon_{L2}$ cannot be recovered and the load with the largest load shedding is disregarded.

iii) If $\Upsilon_{L2} = \varnothing$ and $\Upsilon_{L3} \neq \varnothing$, we disregard partial loads with larger load status in $\Upsilon_{L3}$. For a clear illustration, we analyze the acceleration principle in PDS. Since there is a considerable disparity in load weights in the objective, the high-level loads are recovered in priority and the loads in $\Upsilon^e_{L3}$ are at the same level as $K^{e*}$. Thus, the maximum number of completely restored loads is recorded in (72) and the loads with larger load statuses are disregarded.

$$n^e_{re} = floor\left\{ \left( f^{e*}_{MCRM\text{-}SOCP} - f^{e}_{\varsigma_j=0} \right) / w^{K^{e*}} \right\}, \tag{72}$$

The reason is that if $(n^e_{re}+1)$ loads at the $K^{e*}$ level can be fully recovered, we will formulate the inequality (73) based on $f^{e*}_{MCRM\text{-}SOCP} - f^{e}_{\varsigma_j=0} < (n^e_{re}+1) w^{K^{e*}}$ in (72), which will have a conflict with inequality (70).

$$f(\varsigma) = f^{e*(0)}_{\varsigma_j=0} + (n^e_{re}+1) w^{K^{e*}} > f^{e*}_{MCRM\text{-}SOCP}. \tag{73}$$

Notably, the MCRM-SOCP can guarantee computational accuracy based on the results of Stage 1. The detailed proof of the convergence and global optimality of the load status iterative solution is provided in Appendices A and B.

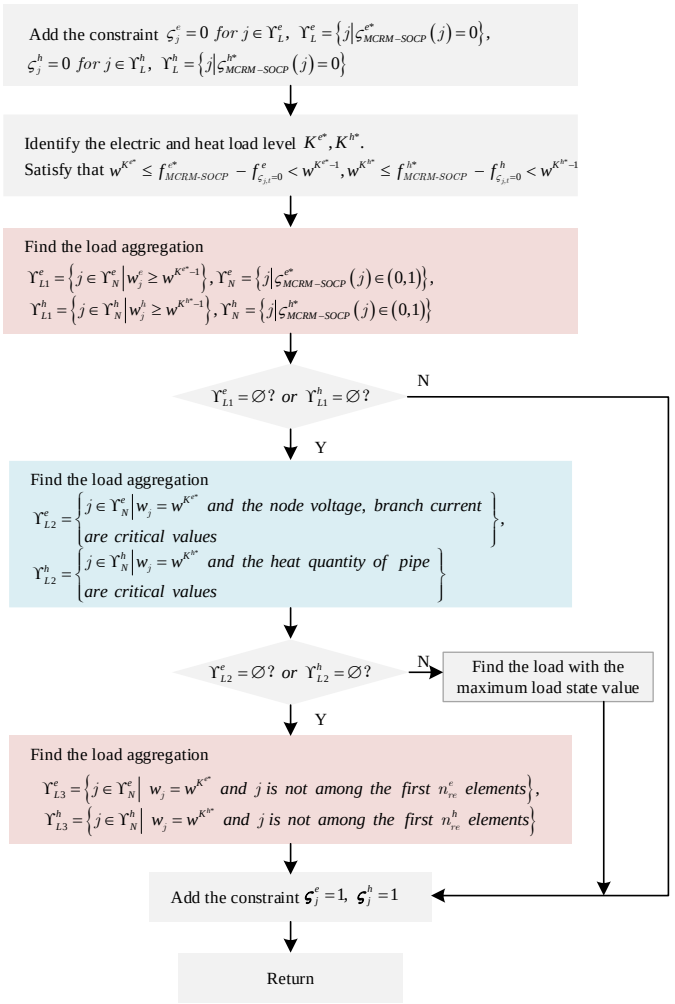


**Fig. 4.** Flowchart of the function A in PDS and DHS.

## V. Case Studies

### A. Case Description

The effectiveness of the coordinated restoration strategy is evaluated using a modified P33H14 system (shown in Fig. 5).

The DHS has installed three heating stations, which equipped with CHP units, EBs, and HBs. Normally, the sectionalizing valves are closed, while the tie valves on pipes PN3-9, PN8-12, and PN9-13 remain open. The DHS network topology is adjusted by open or close these valves as necessary. The DHS/PDS maintenance crews will respectively repair the damaged pipes/lines, where the travel paths will be coordinated to facilitate load restorations.

The electric and heating demands are 1.27 MW+1.03 MVar and 0.77 MW respectively. The DG and CHP unit each possess capacities of 0.5 MVA and 0.5 MW. The specific parameters are listed in [36]. The tests are performed on a desktop workstation configured with an i9-13900K CPU, a Samsung 980 Pro SSD (2TB), and Kingston FURY™ Beast DDR5 RAM at 6000MHz (128GB). MATLAB R2020a is used for programming.

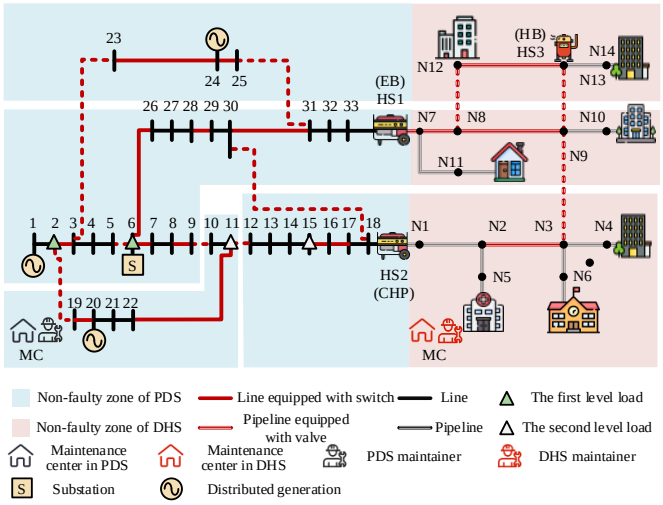


**Fig. 5.** P33H14 system in pre-disaster.

## B. *Efficacy of restoration in the P33H14 test system*

After the catastrophic event, damage is sustained to lines L6-26, L16-17, L23-24, L30-31, and pipes PN2-3, PN9-13, and PN12-13. To assess the impact of coordinated maintenance with reconfiguration on the load restoration of IEHS, three cases are devised.

*Case 1*: Reconfiguration in PDS is utilized and DHS topology remains constant throughout the restoration process. Also, PDS and DHS maintenance crews are separately dispatched to repair the faults.

*Case 2*: PDS and DHS reconfigurations are coordinated, as the PDS and DHS maintenance crews are dispatched respectively.

*Case 3*: PDS and DHS reconfigurations are coordinated and maintenance crews in two subsystems are jointly dispatched for the network restoration.

### 1) *Effect of Coordinated Reconfiguration*

The results of operating the valves and switches are shown in Fig. 6 and load restoration is interpreted in Fig. 7. Table I presents the outcomes of multiperiod load restoration and resilience metrics. The following is a summary of the conclusions reached.

i) The faults in the DHS/PDS can propagate to additional subsystems via their interconnected units, which may result in concurrent energy disruptions in the IEHS. During the fault isolation phase, the electric load curtailment at bus 33 reduces the heat output of the EB in HS1 to zero, which interrupts all heat loads connected to HS1. In the fault isolation stage, the total electrical and heat loads are 0.750 MW and 0.103 MW, which are the same in three Cases.

ii) The coordinated reconfiguration can fully explore the flexibility of network topology for fault recovery. This is achieved through modifications to the DHS network topology in conjunction with PDS switch operations.

In Case 1, the PDS and DHS maintenance crews conduct maintenance to minimize time costs. Since the heating network topology remains constant, electric and heating loads start to be recovered until $t$=30 minutes. The PDS maintenance crew repairs the fault on line L30-31 at $t$=30 minutes, which restores the EB in HS1 connected to bus 33 and supplies the heating loads at N7, N9, and N10.

In Case 2, the DHS maintenance crew repairs the fault on pipe PN2-N3 at $t$=12 minutes. At this time, the transfer of energy is achieved by the valve operation on pipes PN3-9, PN7-8, PN8-9, and PN8-12, which transfer lost heating loads at N3, N4, N6, and N12 to HS2. HS2 is then maximized to ensure the optimal distribution of energy to meet the heating demands. Fig. 7 shows that the load restoration is significantly increased and a shorter time is required to recover all loads.

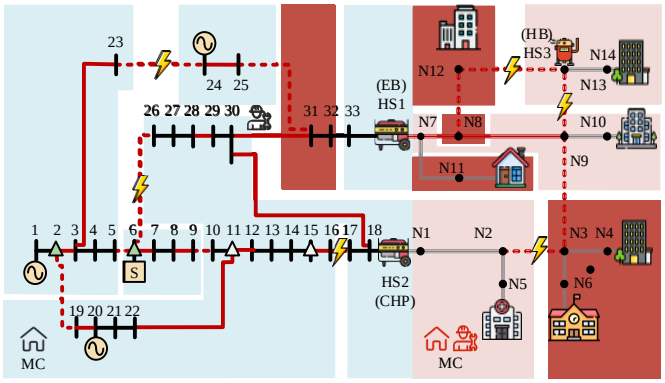

(a) Network topology at $t$=30 min. (Case 1)

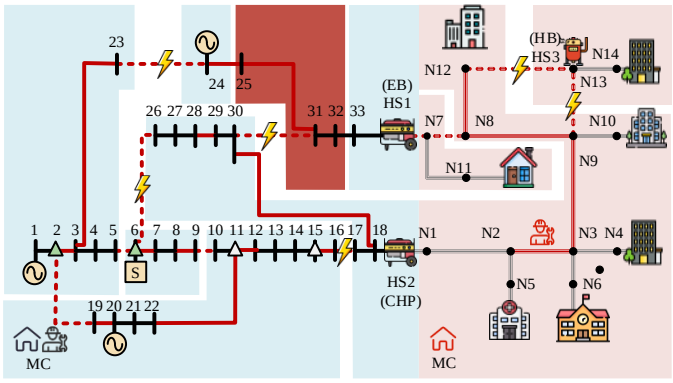

(b) Network topology at $t$=12 min. (Case 2)

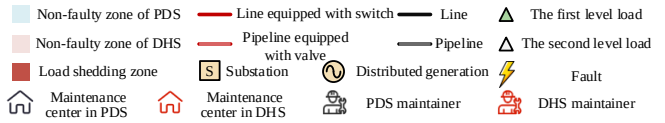


**Fig. 6.** Network topology in the service restoration stage.

TABLE I
MULTIPERIOD LOAD RESTORATION AND RESILIENCE METRICS

| Case | Total load restoration (kW) | Multiperiod restoration (kW) | | Resilience metrics | Restoration time (min.) |
|---|---|---|---|---|---|
| | | Electric | Heat | $R$ | |
| Case 1 | 20558 | 15874 | 4684 | 0.62 | 30 |
| Case 2 | 24810 | 15894 | 8916 | 0.73 | 30 |
| Case 3 | 25758 | 16404 | 9354 | 0.75 | 21 |

iii) Coordinated reconfiguration achieves a better service restoration. As shown in Table I, the overall multiperiod restoration has gone up by 20.7% in Case 2 in comparison to Case 1, and the value of $R$ is increased by 17.7%.

*2) Effect of Coordinated Maintenance*

Table II presents the travel paths for maintenance crews in PDS and DHS and the repair completion time. The summarized conclusions are shown as follows.

i) Coordinated maintenance can redesign the optimal travel paths for the maintenance crews to ensure that essential electrical and heating demands receive energy in a prompt and efficient manner by considering the intricate mutual interaction of PDS and DHS.

In Case 2, PDS and DHS maintenance crews are independently dispatched to achieve fast maintenance of faults in the respective subsystems. DHS maintenance crew repairs the fault on pipe PN2-3 and HS2 can provide greater flexibility in the DHS supply of energy. Then, the PDS maintenance crew repairs the faults on lines L6-26 and L23-24 to reduce maintenance time costs in PDS.

In Case 3, after the fault on pipe PN2-3 is repaired, the PDS maintenance crew repairs the fault on line L30-31 to fast recover the power supply to EB in HS1, so that EB can supply more heating loads on its island, which can provide more flexibility for DHS restoration. Then the fault on line L16-17 is prioritized for maintenance after the fault on pipe PN12-13 is repaired since the CHP unit can provide more operation flexibility to achieve better load restoration.

ii) Coordinated maintenance can entirely provide the flexibility of energy redistribution to ensure a timely energy supply for essential loads, especially when combined with coordinated reconfiguration.

As shown in Table III, in Case 2, at *t*= 21 minutes, the electric loads at buses 25, 31, 32, and 33 are completely lost to ensure the heat output of EB. At this time, EB is powered by DG at bus 24 with restricted capacity.

In Case 3, at *t*= 21 minutes, EB can provide more operation flexibility to supply the electric and heating loads on its island since the faults on pipe PN2-3 and line L30-31 are repaired. The lost heating loads at N3, N4, N6, and N12 are shifted to HS2 by valve operation and EB is powered by the CHP unit by the operation of line L30-31. There is only partial load loss at N12.

iii) In Case 3, the total multiperiod restoration increased by 3.8% in comparison to Case 2, and the value of $R$ is increased by 2.7%. The electric and heating loads will be completely recovered in 21 minutes, earlier than that in Cases 1 and 2 (i.e., in 30 minutes). However, the repair work will be fully completed in 39 minutes, which is slower than that with independent maintenance (i.e., in 33 minutes).

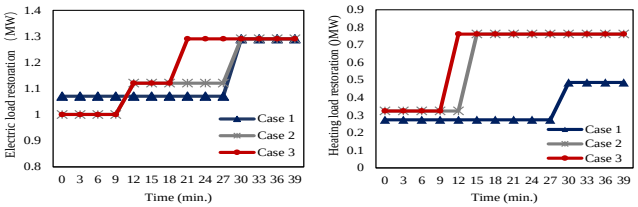


(a) Electric load Restoration (b) Heat load Restoration

**Fig. 7.** Load Restoration in P33H14 system.

TABLE II
REPAIR SEQUENCE AND COMPLETION TIME

| Case | Repair sequence | Repair Completion time (min.) |
|---|---|---|
| Case 1 | PN2-3→L6-26→PN9-13→L23-24 →L30-31→L16-17→PN12-13 | 33 |
| Case 2 | PN2-3→L6-26→PN9-13→L23-24 →L30-31→L16-17→PN12-13 | 33 |
| Case 3 | PN2-3→L30-31→L16-17→PN12-13 →L6-26→L23-24→PN12-13 | 39 |

TABLE III
SWITCH AND VALVE OPERATION AT T= 21 MINUTES

| Line/Pipe | Pre-event stage | Fault isolation stage | Restoration stage | |
|---|---|---|---|---|
| | | | Case 2 | Case 3 |
| PN2-3 | 1 | 0 | 1 | 1 |
| PN12-13 | 1 | 0 | 1 | 1 |
| PN7-8 | 0 | 0 | 0 | 1 |
| L30-31 | 0 | 0 | 0 | 1 |
| L16-17 | 1 | 0 | 0 | 1 |
| L6-26 | 1 | 0 | 1 | 0 |

## C. Efficacy of restoration in the P118H32 test system

The scalability and effectiveness of the coordinated load restoration strategy are evaluated using a large-scale system composed of a 32-node district heating system and a 118-bus power distribution system, with detailed specifications provided in [36]. The system tested includes three CHP units, one heating boiler, three distributed generators, and one substation. It handles heating loads of 2.12 MW and electric loads of 3.31 MW+2.82 MVar. To demonstrate the effectiveness of the proposed dispatch strategy, three cases are executed. Table IV presents the results.

TABLE IV
LOAD RESTORATION AND RESILIENCE METRICS

| Case | Total load restoration (kW) | Multiperiod restoration (kW) | | Resilience metrics | Restoration time (min.) |
|---|---|---|---|---|---|
| | | Electric | Heat | $R$ | |
| Case 1 | 45621 | 30490 | 15131 | 0.64 | 85 |
| Case 2 | 53576 | 30441 | 23135 | 0.71 | 85 |
| Case 3 | 55725 | 30490 | 25235 | 0.73 | 60 |

The incorporation of coordinated maintenance and reconfiguration allows for enhanced load restoration. Specifically, Case 2 demonstrates a 17.4% increase in load restoration compared to Case 1, accompaniedby a 10.9% rise in the value of $R$. In Case 3, load restoration improves by 4.0%, and the resilience metric $R$ increases by 2.8% in comparison to Case 2. Furthermore, the full recovery of both electric and heating loads is achieved within 60 minutes, a faster process

than that achieved with independent maintenance, which takes 85 minutes.

*Analyses of Computational Performance of the TSAA*

The two-stage acceleration algorithm was designed to solve the proposed problem. The numbers of binary variables in P33H14 and P118H32 are 7946 and 12275, respectively. To ascertain the accuracy and efficacy of the proposed algorithm, Table V shows two solutions for comparison. The first solution is entirely based on the Gurobi commercial solver to solve the MRCM, which is called the SBOG. The second solution is the TSAA. The proposed TSAA uses an iterative solution to determine the load status variables. The remaining variables are solved by the Gurobi commercial solver. The commercial solver in the TSAA is illustrated in two stages. In Stage 1, the MCRM-MISOCP is solved by the Gurobi commercial solver. In Stage 2, the load status iterative solution is used to correct or improve the initial outcomes to ensure that the accuracy and efficiency improve the solution of the load statuses. Additionally, the optimal energy flow problem is solved to minimize network losses via the Gurobi commercial solver, which is based on the solution of the load statuses obtained via an iterative algorithm. This process determines the optimal output of the energy sources and ensure an efficient and effective energy distribution in the IEHS.

The proposed algorithm obtained identical total load restoration to Gurobi. In P33H14, the proposed algorithm was approximately 27.14% faster than Gurobi under the default gap of 0.01% in Case 1. In P118H32, the proposed algorithm was approximately 32.45% faster than Gurobi in Case 1. The two-stage acceleration algorithm can be used to solve the multi-period coordinated restoration problem with considerably high efficiency while maintaining the accuracy, which is suitable for fast decision-making.

TABLE V
COMPUTATION PERFORMANCE OF DIFFERENT ALGORITHMS

| System | Case | Computational Time (TSAA/SBOG) | | |
|---|---|---|---|---|
| | | $t_{ave}$ | $t_{min}$ | $t_{max}$ |
| P33H14 | Case 1 | 5.1 s/ 7.0 s | 3.2 s/ 5.3 s | 6.1 s/ 9.4 s |
| | Case 2 | 7.5 s/ 9.7 s | 6.0 s/ 6.6 s | 8.9 s/ 10.5 s |
| | Case 3 | 8.4 s/ 11.6s | 5.2 s/ 8.9 s | 10.3 s/ 13.4 s |
| P118H32 | Case 1 | 10.2 min./ 15.1 min. | 9.1 min./ 10.8 min. | 12.6 min./ 17.4 min. |
| | Case 2 | 11.6 min./ 16.3 min. | 8.5 min./ 15.7 min. | 13.3 min./ 18.5 min. |
| | Case 3 | 12.2 min./ 17.6 min. | 9.3 min./ 16.1 min. | 16.0 min./ 19.2 min. |

## VI. CONCLUSIONS

In this paper, restoration considering the coordinated maintenance and reconfiguration was proposed to enhance the resilience of a park-level IEHS. A two-stage solution algorithm was designed to reduce the computational complexity, which is suitable for fast decision-making in recovery problems. Comprehensive case studies demonstrate that i) the coordinated maintenance of a PDS/DHS is a practical method for restoration by redesigning the optimal travel path for the maintenance crew to ensure that vital loads receive energy on time. ii) The coordinated reconfiguration of the PDS and DHS represents a significant step in the exploration of the potential of varying network topologies for fault recovery. The network structure in the DHS/PDS can be modified to halt greater fault propagation. iii) A two-stage acceleration algorithm was proposed for the fast decision-making of the load restoration problem. The proposed solution can achieve an acceptable level of accuracy while operating at a high level of efficiency.

In future studies, we will conduct comprehensive analyses considering the unbalanced nature of PDSs, random occurrences of pipe/line outages, uncertainties in load demands, and discrepancies in the temporal scales of PDS and DHS in large-scale cities.

## APPENDIX A

The convergence of the load status iterative solution is analyzed as follows: the iterative process will be terminated when $\varsigma^{*}_{MCRM-SOCP}$ only contains integer values. There are finite non-integer values in $\varsigma^{*}_{MCRM-SOCP}$ and the function A will add at least one constant value of $\varsigma^{*}_{MCRM-SOCP}$ in each iteration. Thus, the proposed iterative solution can obtain all values of $\varsigma^{*}_{MCRM-SOCP}$ in a finite number of iterations. The convergence of the load status iterative solution is proven.

## APPENDIX B

To prove the global optimality of the load status iterative solution, it is sufficient to prove that 1) the initially determined load statuses are the optimal solutions; 2) the additional load status based on principles *i*) and *ii*) in each iteration must be identical in the global optimal solution; 3) the processing based on principle *iii*) does not impact the global optimality of the original problem.

For a clear illustration, we analyze the condition in PDS. At first, we prove that the additional load status based on Condition 1) must be optimal. There are two types of loads being analyzed, i.e., the h$^{th}$ level loads satisfying $w^{e}_{h} > w^{K^{e*}}$ and the K$^{th}$ level loads according to $w^{K^{e*}} \le f^{e*}_{MCRM\text{-}SOCP} - f^{e}_{\varsigma_{j,t}=0} < w^{K^{e*}-1}$ in Section IV-B.

For the h$^{th}$ level load, if the load status $\varsigma^{*[1]}_{h}$ is a non-integer value since the node voltage/ branch current is limited and $\varsigma^{*[1]}_{h}$ should be 1 in the global optimal solution. To clarify this, we assume that $\varsigma^{*[1]}_{h} = 0$ and then the other h$^{th}$ level loads and higher-level loads with $\varsigma^{*[1]}_{j} = 0$ cannot be fully restored. The reason is that if all loads are restored, the inequality (74) will be formulated based on $f^{e*}_{MCRM\text{-}SOCP} - f^{e}_{\varsigma_{j,t}=0} < w^{K^{e*}-1}$, which will

conflict with the inequality $f(\varsigma) \le f_{MCRM}^{e*} \le f_{MCRM\text{-}SOCP}^{e*}$ formulated in each iteration.

$$f(\varsigma) = f_{\varsigma_j=0}^{e} + w_j^e \ge f_{\varsigma_j=0}^{e} + w^{K^{e*}-1} > f_{MCRM\text{-}SOCP}^{e*}, \quad j \in \mathrm{N}, \mathrm{N} = \left\{ j | w_j^e \ge w^{K^{e*}-1} \right\}. \tag{74}$$

It means that at least one load status of the h[th] level and higher-level loads should be 1. Considering that $\varsigma_{MCRM\text{-}socp}^{*[1]}$ must ensure the smallest network loss, $\varsigma_h^{*[1]}$ should be 1 in the optimal solution, i.e., $\varsigma_j = \varsigma_j^{*[1]}, j \in \mathrm{I}, \mathrm{I} = \left\{ j | w_j^e > w^{K^{e*}}, \varsigma_j^{*[1]} = 0 \right\}$.

For the K[th] level load with $\varsigma_j^{*[1]} = 0$, $\varsigma_j^{*[1]}$ should be 0 since $\varsigma_{MCRM\text{-}socp}^{*[1]}$ ensures the smallest network loss, i.e., $\varsigma_j = \varsigma_j^*, j \in \mathrm{E}, \mathrm{E} = \left\{ j | w_j^e = w^{K^{e*}}, \varsigma_j^{*[1]} = 0 \right\}$. Thus, condition 1) has been proven.

Conditions 2) and 3) during each iteration have been proved in Section IV-B.

## REFERENCES


[1] S. Yao, P. Wang, X. Liu, H. Zhang, and T. Zhao, "Rolling Optimization of Mobile Energy Storage Fleets for Resilient Service Restoration," *IEEE Trans. Smart Grid*, vol. 11, no. 2, pp. 1030–1043, Mar. 2020.

[2] Y. M. Darestani, A. Shafieezadeh, and R. DesRoches, "Effects of Adjacent Spans and Correlated Failure Events on System-Level Hurricane Reliability of Power Distribution Lines," *IEEE Trans. Power Del*., vol.33, no. 5, p. 10, Oct. 2018.

[3] T. Jiang, T. Sun, G. Liu, X. Li, R. Zhang, and F. Li, "Resilience evaluation and enhancement for island city integrated energy systems", *IEEE Trans. Smart Grid*, vol. 13, no. 4, pp. 2744-2760, 2022.

[4] K. Wang, Y. Xue, Y. Zhou, Z. Li, X. Chang, and H. Sun, "Distributed coordinated reconfiguration with soft open points for resilience-oriented restoration in integrated electric and heating systems," *Appl. Energy*, vol. 365, p. 123207, Jul. 2024.

[5] J. Liu, C. Qin, and Y. Yu, "Enhancing Distribution System Resilience With Proactive Islanding and RCS-Based Fast Fault Isolation and Service Restoration," *IEEE Trans. Smart Grid*, vol. 11, no. 3, pp. 2381–2395, May 2020.

[6] J. Liu, C. Qin, and Y. Yu, "A Comprehensive Resilience-Oriented FLISR Method for Distribution Systems," *IEEE Trans. Smart Grid*, vol. 12, no. 3, pp. 2136–2152, May 2021.

[7] T. Ding, Z. Wang, W. Jia, B. Chen, C. Chen, and M. Shahidehpour, "Multiperiod Distribution System Restoration With Routing Repair Crews, Mobile Electric Vehicles, and Soft-Open-Point Networked Microgrids," *IEEE Trans. Smart Grid*, vol. 11, no. 6, pp. 4795–4808, Nov. 2020.

[8] B. Chen, Z. Ye, C. Chen, J. Wang, T. Ding, and Z. Bie, "Toward a Synthetic Model for Distribution System Restoration and Crew Dispatch," *IEEE Trans. Power Syst.*, vol. 34, no. 3, pp. 2228–2239, May 2019.

[9] S. Lei, C. Chen, Y. Li, and Y. Hou, "Resilient Disaster Recovery Logistics of Distribution Systems: Co-Optimize Service Restoration with Repair Crew and Mobile Power Source Dispatch," *IEEE Trans. Smart Grid*, vol. 10, no. 6, pp. 6187–6202, Nov. 2019.

[10] N. L. Dehghani, Y. M. Darestani, and A. Shafieezadeh, "Optimal lifecycle resilience enhancement of aging power distribution systems: A MINLP-based preventive maintenance planning," *IEEE Access*, vol.8, pp. 22324–22334, 2020.

[11] X. Li, X. Du, T. Jiang, R. Zhang, and H. Chen, "Coordinating multi-energy to improve urban integrated energy system resilience against extreme weather events," *Appl. Energy*, vol. 309, p. 118455, Mar. 2022.

[12] Z. Li, Y. Xu, P. Wang, and G. Xiao, "Coordinated preparation and recovery of a post-disaster Multi-energy distribution system considering thermal inertia and diverse uncertainties," *Appl Energy*, vol. 336, p. 120736, Apr. 2023.

[13] S. D. Manshadi and M. E. Khodayar, "Resilient Operation of Multiple Energy Carrier Microgrids," *IEEE Trans. Smart Grid*, vol. 6, no. 5, pp. 2283–2292, Sep. 2015.

[14] M. Yan, Y. He, M. Shahidehpour, X. Ai, Z. Li, and J. Wen, "Coordinated regional-district operation of integrated energy systems for resilience enhancement in natural disasters", *IEEE Trans. Smart Grid*, vol. 10, no. 5, pp. 4881-4892, Sep. 2019.

[15] G. Li, K. Yan, R. Zhang, T. Jiang, X. Li, and H. Chen, "Resilience-Oriented Distributed Load Restoration Method for Integrated Power Distribution and Natural Gas Systems," *IEEE Trans. Sustain. Energy*, vol. 13, no. 1, pp. 341–352, Jan. 2022.

[16] Y. Lin, B. Chen, J. Wang, and Z. Bie, "A Combined Repair Crew Dispatch Problem for Resilient Electric and Natural Gas System Considering Reconfiguration and DG Islanding," *IEEE Trans. Power Syst.*, vol. 34, no. 4, pp. 2755–2767, Jul. 2019.

[17] "Flexibility Improvement of Power Systems: Technical Paths, Economies, and Policy Recommendations" [Online]. Available: http://www.nrdc.cn/Public/uploads/2022-07-18/62d4c2e313df1.pdf

[18] K. Wang, Y. Xue, Q. Guo, M. Shahidehpour, Q. Zhou, B. Wang, and H. Sun, "A Coordinated Reconfiguration Strategy for Multi-Stage Resilience Enhancement in Integrated Power Distribution and Heating Networks," *IEEE Trans. Smart Grid*, vol. 14, no. 4, pp. 2709–2722, Jul. 2023.

[19] Z. Li, Y. Xu, P. Wang, and G. Xiao, "Restoration of Multi Energy Distribution Systems With Joint District Network Recon Figuration by a Distributed Stochastic Programming Approach," *IEEE Trans. Smart Grid*, (early access), 2023.

[20] M. Khatibi, J. D. Bendtsen, J. Stoustrup, and T. Molbak, "Exploiting power-to-heat assets in district heating networks to regulate electric power network," *IEEE Trans. Smart Grid*, vol. 12, no. 3, pp. 2048–2059, May 2021.

[21] Y. Liu, Y. Su, Y. Xiang, J. Liu, L. Wang, and W. Xu, "Operational reliability assessment for gas-electric integrated distribution feeders," *IEEE Trans. Smart Grid*, vol. 10, no. 1, pp. 1091–1100, Jan. 2019.

[22] D. Mao, P. Wang, W. Wang, and L. Ni, "Reliability segment design in single-source district heating networks based on valve network models," *Sustainable Cities and Society*, vol. 63, p. 102463, Dec. 2020.

[23] M. Kordestani, A. Zanj, M. E. Orchard, and M. Saif, "A modular fault diagnosis and prognosis method for hydro-control valve system based on redundancy in multisensor data information," *IEEE Trans. Rel*., vol. 68, no. 1, pp. 330–341, Mar. 2019.

[24] X. Wang, N. H. El-Farra, and A. Palazoglu, "Proactive reconfiguration of heat-exchanger supernetworks," *Ind. Eng. Chem. Res.*, vol. 54, no. 37, pp. 9178–9190, Sep. 2015.

[25] T. Bektas, "The multiple traveling salesman problem: An overview of formulations and solution procedures," *Omega*, vol. 34, no. 3, pp. 209–219, Jun. 2006.

[26] Y. Lin, B. Chen, J. Wang, and Z. Bie, "A Combined Repair Crew Dispatch Problem for Resilient Electric and Natural Gas System Considering Reconfiguration and DG Islanding", *IEEE Trans. Power Syst.*, vol. 34, no. 4, pp. 2755–2767, Jul. 2019.

[27] R. Cheng, Z. Wang, and Y. Guo, "An online feedback-based linearized power flow model for unbalanced distribution networks," *IEEE Trans. Power Syst.*, vol. 37, no. 5, pp. 3552–3565, Sep. 2022.

[28] D. Zhu, B. Yang, Y. Liu, Z. Wang, K. Ma, and X. Guan, "Energy management based on multi-agent deep reinforcement learning for a multi-energy industrial park," *Appl. Energy*, vol. 311, Apr. 2022, Art. no. 118636.

[29] Y. Wang, Y. Xu, J. Li, J. He, and X. Wang, "On the Radiality Constraints for Distribution System Restoration and Reconfiguration Problems," *IEEE Trans. Power Syst.*, vol. 35, no. 4, pp. 3294–3296, Jul. 2020.

[30] Y. Xue, M. Shahidehpour, Z. Pan, B. Wang, Q. Zhou, Q. Guo, and H. Sun, "Reconfiguration of district heating network for operational flexibility enhancement in power system unit commitment," *IEEE Trans. Sustain. Energy*, vol. 12, no. 2, pp. 1161–1173, Apr. 2021.

[31] M. Farivar and S. H. Low, "Branch flow model: Relaxations and convexification—Part I," *IEEE Trans. Power Syst.*, vol. 28, no. 3, pp. 2554–2564, Aug. 2013.

[32] Yinbiao Shu, "Planning design of distribution networks," China Electric Power Press, 2018:146.

[33] Y. Li, J. Xiao, C. Chen, Y. Tan, and Y. Cao, "Service Restoration Model With Mixed-Integer Second-Order Cone Programming for Distribution Network With Distributed Generations," *IEEE Trans. Smart Grid*, vol. 10, no. 4, pp. 4138–4150, Jul. 2019.

[34] G. Li, K. Yan, R. Zhang, T. Jiang, X. Li, and H. Chen, 'Resilience-Oriented Distributed Load Restoration Method for Integrated Power Distribution and Natural Gas Systems', *IEEE Trans. Sustain. Energy*, vol. 13, no. 1, pp. 341–352, Jan. 2022.
[35] Y. Wang, Y. Xu, J. He, C. -C. Liu, K. P. Schneider, M. Hong, D. T. Ton., "Coordinating Multiple Sources for Service Restoration to Enhance Resilience of Distribution Systems," *IEEE Transactions on Smart Grid*, vol. 10, no. 5, pp. 5781-5793, Sept. 2019.
[36] " Test data of maintenance crew scheduling considering the optimal reconfiguration in Matlab format", 2024. [Online].Available: https://docs.google.com/file/d/1p0Nw4To6etRNIO4c2mJdjXxAhRHmosJP/edit?usp=docslist_api&filetype=msexcel

**Ke Wang** (Student Member, IEEE) received the B.S. degree from Hefei University of Technology, Hefei, China. She is currently pursuing the Ph.D. degree with the College of Electrical and Power Engineering, Taiyuan University of Technology, Taiyuan, China. Her research interests include resilience enhancement in integrated power distribution and heating systems.

**Yixun Xue** (Member, IEEE) received Ph.D. degrees from Tsinghua University, in 2021. In 2021, he joined Taiyuan University of Technology, Taiyuan, China, where he is currently an Associate Professor. His research interests include coordinated planning and optimization, and resilience enhancement in integrated energy systems.

**Mohammad Shahidehpour** (Life Fellow, IEEE) received the Honorary Doctorate degree in electrical engineering from the Polytechnic University of Bucharest, Bucharest, Romania. He is the Bodine Chair Professor and the Director of Robert W. Galvin Center for Electricity Innovation with IIT, Chicago, USA. He is a Fellow of the American Association for the Advancement of Science, National Academy of Inventors, a Laureate of Khwarizmi International Award, and an Elected Member of the U.S. National Academy of Engineering. He is listed on the Web of Science as a highly cited researcher.

**Xinyue Chang** (Member, IEEE) received the Ph.D. degrees in electrical engineering from Tsinghua University, Beijing, China, in 2022. She is currently an Associate Professor at Taiyuan University of Technology, Taiyuan, China. Her current research interests include distributed optimization, robust, and stochastic optimization of smart grids.

**Zening Li** (Member, IEEE) received the Ph.D. degree in Electrical Engineering from Beijing Jiaotong University, Beijing, China, in 2022. He is currently a lecturer at Taiyuan University of Technology, Taiyuan, China. His research interests include smart building, active distribution network, and integrated energy system.

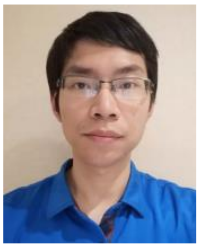

**Yue Zhou** (Member, IEEE) received the Ph.D. degree in Electrical Engineering from Tianjin University, Tianjin, China, in 2016. He is currently a Lecturer in cyber–physical systems with the School of Engineering, Cardiff University, Cardiff, U.K. His research interests include demand response, peer-to-peer energy trading, and cyber–physical systems.

**Hongbin Sun** (Fellow, IEEE) received the double B.S. degrees from Tsinghua University in 1992, the Ph.D. degree from the Department of Electrical Engineering, Tsinghua University, in 1996. He is currently the Vice Chancellor of Taiyuan University of Technology and the ChangJiang Scholar Distinguished Professor of Tsinghua University. He is a Member of the Academic Committee of Tsinghua University, the Chief Scientist of Major Science and Technology Infrastructure of Shanxi Energy Internet, the Chief Scientist in Polar Clean Energy of Polar Research Institute of China, the National Distinguished Teacher, and the Fellow of IEEE/IET/CSEE. He is also a Member of IEEE PES Fellow Evaluation Committee, the Vice Chair of Energy Committee of WFEO, the Inaugural Chair of IEEE PES Energy Internet Coordinating Committee, the Founding Chairman of IEEE Conference on Energy Internet and the Energy System Integration, and the Founding Editor-in-Chief of Energy Internet Journal. He has been awarded over ¥80M research grants as the principal investigator, such as the National Program on Key Basic Research Project (973 Program), the National High-tech R&D Program of China (863 Program), the National Key Research and Development Program of China, and the National Natural Science Foundation of China (Key Program, Integration Program). He has won the first prize in the National Science and Technology Progress Award, and the second prize in the National Technology Invention Award. His achievements have been featured twice in Chinese Universities Top Ten Great Scientific and Technological Progresses. He has also won two times of the first prize in the National High Education Achievement Award. In addition, he was awarded the Inaugural Energy Internet Pioneer Award in 2020 and the Asia Pacific Federation of Engineering Organizations Engineer Award in 2022. He is also a highly cited Chinese scholar (2020-2022) in Elsevier. He has published more than 200 SCI papers and 5 books, which have more than 6,750 SCI citations and more than 20,000 Google citations. He has been authorized 40 US Patents of Invention and more than 200 Chinese Patents of Invention.